Delft University of Technology

Properties of sputtered $BaSi_2$ thin films annealed in vacuum condition

Tian, Yilei; Montes, Ana Rita; Vančo, Ľubomír; Isabella, Olindo; Zeman, Miro

DOI
10.7567/1347-4065/ab5b59

Publication date
2020

Document Version
Final published version

Published in
Japanese Journal of Applied Physics

Citation (APA)
Tian, Y., Montes, A. R., Vančo, Ľ., Isabella, O., & Zeman, M. (2020). Properties of sputtered $BaSi_2$ thin films annealed in vacuum condition. *Japanese Journal of Applied Physics*, *59*(SF), SFFA03-1 - SFFA03-4. Article SFFA03. https://doi.org/10.7567/1347-4065/ab5b59

Important note
To cite this publication, please use the final published version (if applicable).
Please check the document version above.

Copyright
Other than for strictly personal use, it is not permitted to download, forward or distribute the text or part of it, without the consent of the author(s) and/or copyright holder(s), unless the work is under an open content license such as Creative Commons.

Takedown policy
Please contact us and provide details if you believe this document breaches copyrights.
We will remove access to the work immediately and investigate your claim.

This work is downloaded from Delft University of Technology.
For technical reasons the number of authors shown on this cover page is limited to a maximum of 10.

Japanese Journal of Applied
Physics

The Japan Society
of Applied Physics

REGULAR PAPER

Properties of sputtered $BaSi_2$ thin films annealed in vacuum condition

To cite this article: Yilei Tian *et al* 2020 *Jpn. J. Appl. Phys.* **59** SFFA03

View the article online for updates and enhancements.

This content was downloaded from IP address 145.94.75.32 on 28/04/2020 at 16:31

Japanese Journal of Applied Physics **59**, SFFA03 (2020) **REGULAR PAPER**
https://doi.org/10.7567/1347-4065/ab5b59

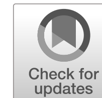

Properties of sputtered $BaSi_2$ thin films annealed in vacuum condition

Yilei Tian[1*], Ana Rita Montes[1,2], Ľubomír Vančo[3], Olindo Isabella[1*], and Miro Zeman[1]

[1]*Photovoltaic Materials and Devices group, Delft University of Technology, Delft, 2628 CD, The Netherlands*
[2]*Faculty of Sciences, University of Lisbon, Lisbon, 1749-016, Portugal*
[3]*University Science Park Bratislava Centre, Slovak University of Technology in Bratislava, Bratislava, 812 43, Slovakia*

[*]E-mail: y.tian@tudelft.nl; o.isabella@tudelft.nl

Received September 27, 2019; revised October 14, 2019; accepted November 25, 2019; published online January 17, 2020

As a potential absorber candidate for high-efficient solar cell applications, $BaSi_2$ films are confronted with issues of surface oxidation associated with the high-temperature annealing. Herein, $BaSi_2$ films are deposited by the sputtering technique. A vacuum annealing process is subsequently carried out to crystallize sputtered $BaSi_2$ films. Raman spectroscopy is used to study surface structures and crystalline quality. Elemental depth profile is measured by Auger Electron spectroscopy to understand the compositions of films. Optical and electrical properties are further investigated to reveal the effects of annealing condition. Applying vacuum annealing condition can effectively suppress diffusions of Ba and ensures a stochiometric $BaSi_2$ layer. However, surface oxidation still occurs even in the vacuum environment owing to the high reactivity of Ba. Further attempts to prevent $BaSi_2$ surface oxidation may focus on the combination of other methods, such as capping layer and reducing atmosphere, with vacuum (or low-pressure) annealing condition. © 2020 The Japan Society of Applied Physics

1. Introduction

$BaSi_2$ is emerging as a promising light-absorbing material toward high-performance photovoltaic (PV) solar cell applications.[1,2] $BaSi_2$ is stable in the ambient condition,[3] exhibits an unintentionally n-type conductivity,[4] and possesses a suitable band gap ($E_g = \sim 1.3$ eV) for solar energy conversion.[5–8] Besides, it holds attractive optical and electrical properties, including a high light absorption coefficient (α) reaching 10^5 cm^{-1} for photon energy $h\nu > 1.5$ eV,[9,10] a long minority carrier lifetime τ($\sim$10–27 μs),[11–13] and essentially elemental abundance and non-toxicity. The theoretical conversion efficiency (η) of $BaSi_2$ homojunction solar cells can be up to 25%.[1] Currently, the experimental efficiency of $BaSi_2$/Si heterojunction solar cells reaches 9.9%.[14] High-quality $BaSi_2$ films for solar cell applications have been fabricated by molecular beam epitaxy.[14,15] Great efforts have been put into developments of low-cost deposition method of $BaSi_2$, such as chemical vapor deposition technique,[16] thermal evaporation,[8,17–19] and sputtering.[20–22] Among them, sputtering is an industrially applicable technique, enabling high deposition rates and large-scale depositions. Besides, it ensures an excellent stoichiometry control for compound material depositions. $BaSi_2$ films have be deposited by sputtering either at room temperature or at high temperatures up to 600 °C.[23,24] The room temperature sputtering process has less strict requirements on the heating system of deposition equipment, enabling its facile industrial deployment.

However, $BaSi_2$ sputtered at room temperature is always associated with high-temperature annealing for crystallization. And issues related to high-temperature annealing, such the surface oxidation and the associated Ba diffusion, hinder the development of sputtered $BaSi_2$.[20] To alleviate those issues, some attempts can be tried, including $BaSi_2$ sample architecture redesign, oxide layer etching, and annealing condition controlling. Capping layer, such as a-Si, can be employed to change the sample architecture and to prevent surface oxidation.[14,25,26] However, reactions between the additional layer and $BaSi_2$ may introduce other issues and increase the difficulties of film quality control.[25] In respect to etching, the high reactivity of $BaSi_2$ definitely increases the complexity of both wet- and dry-etching method developments. Controlling the annealing condition is relatively a facile strategy. The $BaSi_2$ film, annealed at N_2 atmosphere with the existing of residual O_2, presents a thick oxide layer around 200 nm, and a Si-rich composition.[20] By reducing the oxygen content or introducing the reducing atmosphere, the surface oxidation and Ba diffusion may be effectively suppressed.

Herein, we present the effects of high-vacuum annealing conditions on the properties of $BaSi_2$ films. $BaSi_2$ thin films are deposited through sputtering processes and are subsequently annealed in a high-vacuum environment. Structural, optical, and electrical properties are characterized to investigate the influences of annealing conditions. Employing a high-vacuum annealing environment can effectively alleviate Ba diffusion and improve stoichiometry of $BaSi_2$ layer. However, the surface oxidation cannot be effectively avoided, thus other anti-oxidation strategies need to be attempted. This research shed light on the optimization of $BaSi_2$ annealing methods. Combining it with other anti-oxidation annealing strategies may help with developing high-quality $BaSi_2$ films and high-efficient solar cells.[27–30]

2. Experimental methods

$BaSi_2$ films were deposited in a radio-frequency magnetron sputtering setup (Kurt J. Lesker) with a stoichiometric ceramic $BaSi_2$ target. Prior to the depositions, the target was cleaned by a pre-sputtering. Sputtering processes were executed with an Ar gas flow at room temperature. Plasma power and deposition pressure were set as 50 W and 10 μbar, respectively. Subsequent annealing was conducted at temperatures ranging from 550 °C to 630 °C in high-vacuum ($<10^{-3}$ μbar) environment.

Raman spectra were recorded on a Renishaw InVia™ confocal Raman microscope with 633 nm laser excitation. Elemental composition analysis was carried out in Jeol JAMP 9510-F Auger Microprobe at 10 keV energy with a tilt angle of 30°. During sputtering cycles, 1000 eV Ar^+ ions were utilized. Reflectance and transmittance were obtained on a Perkin Elmer Lambda 950 UV–vis-NIR spectrometer single beam instrument over a range of 300–2500 nm. Absorptance was calculated by absorptance (%) = 100% − reflectance

 © 2020 The Japan Society of Applied Physics

(%) − transmittance (%). Resistivity and Hall effect measurements were conducted with van der Pauw geometry. Al contacts were deposited by vacuum thermal evaporation (PRO500S, Provac). Samples were subsequently annealed at 130 °C for 30 min to ensure ohmic contacts.

3. Results and discussion

Figure 1 presents Raman spectra of $BaSi_2$ annealing in vacuum at different temperatures, namely 550 °C, 575 °C, 600 °C, and 630 °C. Annealing durations are kept the same for 30 min. Raman signatures of $BaSi_2$ can be observed in all spectra, suggesting the existence of crystalline phase of $BaSi_2$ in all samples.[31] Crystallization of sputtered $BaSi_2$ can be achieved at lower annealing temperatures in *vacuo* than in N_2 atmosphere. Obvious $BaSi_2$ vibration bands can be observed even in the sample annealed at 550 °C, while no distinguishable peaks can be found with samples annealed at the same temperature in N_2.[20] The vacuum condition can decrease the thermal budget for $BaSi_2$ crystallization. And in this condition, the sample annealed at 600 °C has already exhibited a rather sharp Raman spectrum.

However, non-uniform surfaces are observed with all the samples, displayed by the optical microscopy images in Fig.1. At a lower annealing temperature, such as 550 °C, the brownish region (point A1) holds a Raman spectrum presenting strong $BaSi_2$ bands together with a peak at 519 cm^{-1} associated to Si nanocrystals (NCs). The existence of Si NCs is the consequence of surface oxidation.[20] Hence, the composition of region A1 can be a mixture of $BaSi_2$, Si NCs, and other oxidation by-products. It should be addressed that the surface oxidation still occurs during the annealing process of $BaSi_2$ even in the high-vacuum condition. This can be due to the high reactivity between $BaSi_2$ with residual oxygen (extremely low content considering the pressure in the scale of 10^{-3} μbar) in the annealing chamber. Besides, a weak peak at around 245 cm^{-1} can also be noticed. The intensity of this peak is much higher in the Raman spectrum of point B1 of the other region. On the other hand, $BaSi_2$ peaks are less distinguishable in the point B1. It suggests a low degree of crystallization of $BaSi_2$. Interestingly, no Si peak is detected in the B1 region, indicating it is less oxidized. Hence, the peak at 245 cm^{-1} may be attributed to other Ba–Si(–O) compounds, which are inclined to be formed rather than $BaSi_2$ at a lower temperature. In summary, $BaSi_2$ annealed at a lower temperature (550 °C) is partially oxidized, containing Si NCs and other Ba–Si(–O) compounds. And in such condition, $BaSi_2$ is not fully crystallized, leaving some amorphous phase.

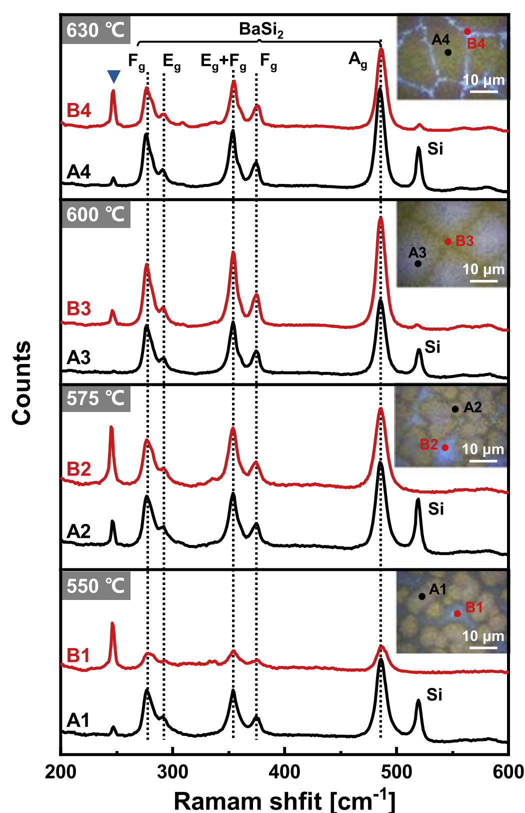

Fig. 1. (Color online) Raman spectra of $BaSi_2$ annealed in vacuum at temperatures of 550 °C, 575 °C, 600 °C, and 630 °C. Inserts are optical microscopy images captured by the Raman setup.

By increasing temperature to 575 °C, two different regions in the surface can still be observed. Obvious $BaSi_2$ peaks can be noticed in both regions. This indicates an enhancement of $BaSi_2$ crystallization due to the increase of annealing temperature. In case of 600 °C, the surface appearance changes a lot from cases of 550 °C and 575 °C. Larger grains (with a color of light blue) are formed, as shown by the microscopy images in Fig.1. In the grain region, the Raman spectrum of point A3 contains no peak at 245 cm^{-1}, while the spectrum of point B3 in the boundary region exhibits a pretty weak Si peak, together with a weaker peak at 245 cm^{-1} comparing to B1 and B2. The annealing temperature of 600 ° C may either avoid the formation of other Ba–Si(–O) compounds or promote the transition of these compounds to other compositions, which cannot be detected by Raman. When further increasing the temperature to 630 °C, which is the limit of the annealing equipment, more distinguishable regions can be noticed in the microscopy images. And a stronger peak at 245 cm^{-1} is displayed by the spectrum of point B4 in the boundary region. Therefore, temperature around 600 °C can be enough to crystallize $BaSi_2$ at vacuum according to Raman spectroscopy, which is lower than the annealing temperature of 650 °C in N_2 atmosphere.[20]

The samples annealed for longer durations have also been investigated. Figure 2 exhibits Raman spectra of $BaSi_2$ films annealed at 600 °C for 30, 60, and 90 min. Prolonging the annealing duration from 30 to 60 min leads to few differences in Raman spectra. However, an obvious surface morphology change can be noticed. Boundary regions (B3) disappears in the surface of the sample annealed for 60 min. Further extending the duration to 90 min results in a surface which is more uniform. And Raman spectra of all regions in the samples annealed for 90 min contain strong Si peaks as well as peaks at 245 cm^{-1}. Hence, such uniformity enhancement of the surface can be a consequence of deeper surface oxidation. Longer annealing duration allows residual oxygen to react at $BaSi_2$ film surface during annealing. In summary, prolonging annealing cannot significantly improve $BaSi_2$ quality, but rather promotes the surface oxidation.

Raman spectroscopy only reflects the surface structure information. Auger electron spectroscopy was employed to investigate the atomic concentration depth profiles. The atomic concentration depth profile of $BaSi_2$ annealed at 600 °C for 30 min is depicted in Fig. 3(a). There is an oxide

 © 2020 The Japan Society of Applied Physics

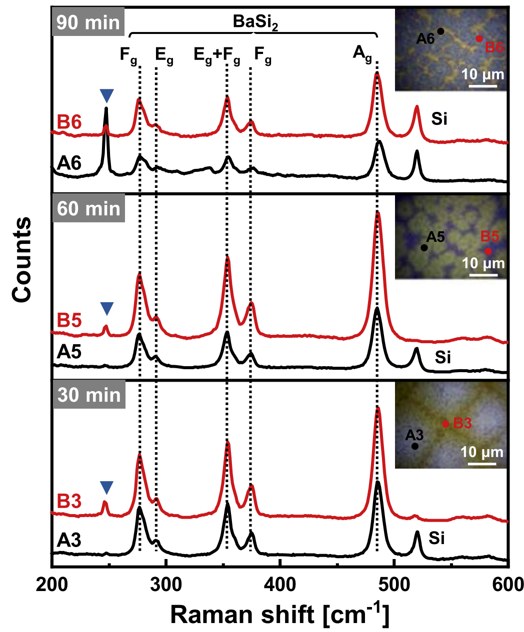

Fig. 2. (Color online) Raman spectra of $BaSi_2$ films annealed at 600 °C for 30, 60, and 90 min.

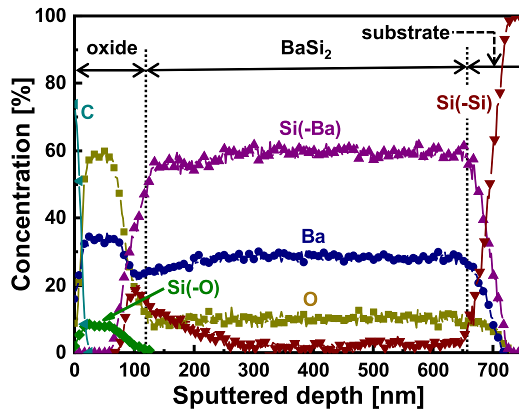

Fig. 3. (Color online) Elemental concentration depth profiles of $BaSi_2$ annealed at 600 °C for 30 min Si bonded with O, Ba, and Si are denoted as Si (–O), Si(–Ba), and Si(–Si), respectively.

layer on the surface, which mainly consists of SiO_x and BaO. A trace of carbon is also detected, which may originate from residual CO_2 in the annealing chamber. The surface oxidation of $BaSi_2$ in high-temperature can be hardly prevented even by employing a high-vacuum environment. The relatively high reactivity of barium enables interactions even with extremely low-concentration residual O_2 and CO_2 in the chamber. Nevertheless, the high-vacuum annealing reduces the oxide layer thickness from ~200 nm (annealed in N_2 atmosphere) to ~100 nm.[20] Meanwhile, the $BaSi_2$ layer holds a good stoichiometry, with a Ba:Si ratio of 1:2. Fewer Ba atoms diffuse to surface or substrate. Oxygen is the cause driving the diffusion of Ba. By reducing the content of oxygen, the diffusion of Ba is suppressed, preventing a drastic structural transformation of $BaSi_2$ films.

The optical and electrical properties of $BaSi_2$ annealing in vacuum were further characterized. Figure 4 shows the absorptance curves of $BaSi_2$ annealed at 550 °C–630 °C. A slight increase of ultraviolet-visible absorptance can be noticed with the increase of annealing temperature.

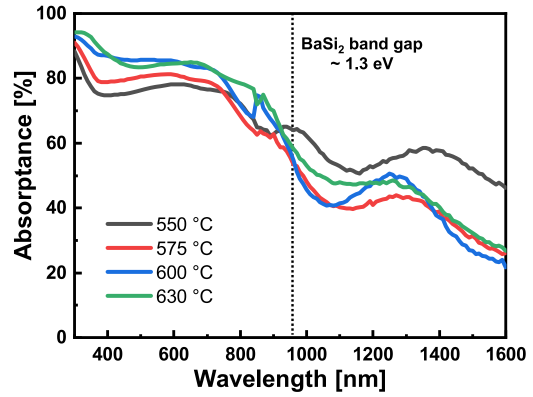

Fig. 4. (Color online) Absorptance curves of $BaSi_2$ films annealed at 550 °C, 575 °C, 600 °C, and 630 °C.

However, all samples display strong infrared absorptance where the photon energy is lower than $BaSi_2$ band gap around 1.3 eV.[4] The infrared absorptance can be reduced by increasing the annealing temperature. When the annealing temperature reaches to 575 °C, the infrared absorptance does not significantly decrease. This is most likely related to the presence of band-gap states resulted from detective phases or impurities. Combining with Raman spectra, the lower temperature can hardly induce a full crystallization of $BaSi_2$. Defects in the film could cause the band gap states and result in this infrared absorptance. Higher annealing temperatures could reduce the defective phases and alleviate such absorptance below the band gap.

Hall effect measurements were conducted to determine carrier type and concentrations. As shown in Fig. 5, $BaSi_2$ films annealed at lower temperatures, namely 550 °C and 575 °C, randomly present n or p carrier types. Owing to the presence of a high volume of impurities and amorphous phases, samples may not have specific conduction type. By enhancing the annealing temperature, a constant sign of carrier type can be observed. The sample annealed at 600 °C exhibits an n-type nature, with an average electron carrier concentration of 3.01×10^{17} cm^{-3}. The sample annealed at 630 °C possesses an even lower average electron carrier concentration of 1.52×10^{17} cm^{-3}. A higher annealing temperature can improve the crystallinity and reduce the vacancy defects in the film. Consequently, the carrier concentration would decrease. Interestingly, for increasing annealing temperature, an overall decreasing trend of carrier

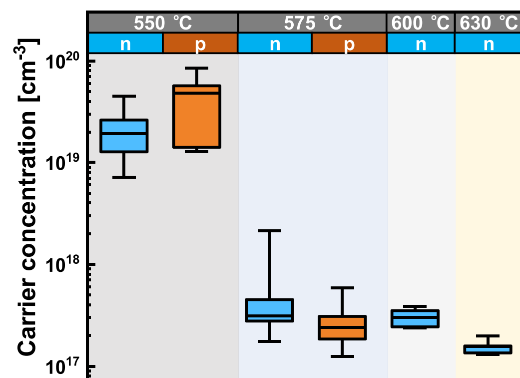

Fig. 5. (Color online) Carrier concentrations in $BaSi_2$ films annealed at 550 °C, 575 °C, 600 °C, and 630 °C.

© 2020 The Japan Society of Applied Physics

concentration magnitude is observed, despite the unpredictable carrier type in cases of 550 °C and 575 °C.

4. Conclusions

In summary, this work investigated the effects of vacuum annealing condition on the properties of sputtered $BaSi_2$ films. Employing the vacuum condition can alleviate the diffusion of Ba, thus ensuring a stoichiometric $BaSi_2$ layer. Despite the fact that surface oxidation still occurs during vacuum annealing, the thickness of the oxide layer is reduced as compared to the case of N_2 atmosphere annealing. Moreover, increasing annealing temperature can reduce the defective phases and enhance the crystalline quality of $BaSi_2$. The drop of infrared absorptance and decrease carrier concentration can be noticed as results of decrease of defects. The annealing temperature of 600 °C with a duration of 30 min is sufficient to promote the $BaSi_2$ crystallization in *vacuo*. Further research is still required to establish the method for achieving PV-grade sputtered $BaSi_2$ films, with limited surface oxidation and fewer defects or impurities.

Acknowledgments

The authors would like to thank Martijn Tijssen and Stefaan G.M. Heirman for daily technical equipment support. Y.T. thanks financial support from the China Scholarship Council. A.M. acknowledges financial support by the MIT Portugal program and the Fundação para a Ciência e a Tecnologia (FCT).

1) T. Suemasu, Jpn. J. Appl. Phys. **54**, 07JA01 (2015).
2) T. Suemasu and N. Usami, J. Phys. D: Appl. Phys. **50**, 023001 (2016).
3) H. Schäfer, K. Janzon, and A. Weiss, Angew. Chem. Int. Ed. **2**, 393 (1963).
4) K. Morita, Y. Inomata, and T. Suemasu, Thin Solid Films **508**, 363 (2006).
5) T. Nishii, T. Mizuno, Y. Mori, K. Takarabe, M. Imai, and S. Kohara, Phys. Status Solidi B **244**, 270 (2007).
6) M. Kumar, N. Umezawa, and M. Imai, Appl. Phys. Express **7**, 071203 (2014).
7) M. Kumar, N. Umezawa, and M. Imai, J. Appl. Phys. **115**, 203718 (2014).
8) K. O. Hara, Y. Nakagawa, T. Suemasu, and N. Usami, Jpn. J. Appl. Phys. **54**, 07JE02 (2015).
9) K. Toh, T. Saito, and T. Suemasu, Jpn. J. Appl. Phys. **50**, 068001 (2011).
10) W. Du, R. Takabe, S. Yachi, K. Toko, and T. Suemasu, Thin Solid Films **629**, 17 (2017).
11) K. O. Hara, N. Usami, K. Nakamura, R. Takabe, M. Baba, K. Toko, and T. Suemasu, Appl. Phys. Express. **6**, 112302 (2013).
12) R. Takabe, K. O. Hara, M. Baba, W. Du, N. Shimada, K. Toko, N. Usami, and T. Suemasu, J. Appl. Phys. **115**, 193510 (2014).
13) N. Shaalan, K. Hara, C. Trinh, Y. Nakagawa, and N. Usami, Mater. Sci. Semicond. Process. **76**, 37 (2018).
14) S. Yachi, R. Takabe, H. Takeuchi, K. Toko, and T. Suemasu, Appl. Phys. Lett. **109**, 072103 (2016).
15) D. Tsukahara, S. Yachi, H. Takeuchi, R. Takabe, W. Du, M. Baba, Y. Li, K. Toko, N. Usami, and T. Suemasu, Appl. Phys. Lett. **108**, 152101 (2016).
16) A. Pokhrel, L. Samad, F. Meng, and S. Jin, Nanoscale **7**, 17450 (2015).
17) K. O. Hara, J. Yamanaka, K. Arimoto, K. Nakagawa, T. Suemasu, and N. Usami, Thin Solid Films **595**, 68 (2015).
18) Y. Nakagawa, K. O. Hara, T. Suemasu, and N. Usami, Jpn. J. Appl. Phys. **54**, 08KC03 (2015).
19) K. O. Hara, C. Yamamoto, J. Yamanaka, K. Arimoto, K. Nakagawa, and N. Usami, Jpn. J. Appl. Phys. **57**, 04FS01 (2018).
20) Y. Tian, R. Vismara, S. Van Doorene, P. Šutta, L. U. Vančo, M. Vesely, P. Vogrinčič, O. Isabella, and M. Zeman, ACS Appl. Energy Mater. **1**, 3267 (2018).
21) T. Yoneyama, A. Okada, M. Suzuno, T. Shibutami, K. Matsumaru, N. Saito, N. Yoshizawa, K. Toko, and T. Suemasu, Thin Solid Films **534**, 116 (2013).
22) N. A. A. Latiff, T. Yoneyama, T. Shibutami, K. Matsumaru, K. Toko, and T. Suemasu, Phys. Status Solidi C **10**, 1759 (2013).
23) A. Sasaki, Y. Kataoka, K. Aoki, S. Saito, K. Kobayashi, T. Ito, K. Kakushima, and H. Iwai, Jpn. J. Appl. Phys. **54**, 031202 (2015).
24) S. Matsuno, T. Nemoto, M. Mesuda, H. Kuramochi, T. Kaoru, and T. Suemasu, Appl. Phys. Express **12**, 021004 (2019).
25) Y. Tian, A. Montes, O. Isabella, and M. Zeman, 12th Int. Conf. on Advanced Semiconductor Devices and Microsystems (ASDAM), 2018, p. 1.
26) K. O. Hara, C. T. Trinh, Y. Kurokawa, K. Arimoto, J. Yamanaka, K. Nakagawa, and N. Usami, Thin Solid Films **636**, 546 (2017).
27) T. Saito, D. Tsukada, Y. Matsumoto, R. Sasaki, M. Takeishi, T. Ootsuka, and T. Suemasu, Jpn. J. Appl. Phys. **48**, 106507 (2009).
28) W. Du, R. Takabe, M. Baba, H. Takeuchi, K. Hara, K. Toko, N. Usami, and T. Suemasu, Appl. Phys. Lett. **106**, 122104 (2015).
29) K. Takahashi, Y. Nakagawa, K. O. Hara, Y. Kurokawa, and N. Usami, Jpn. J. Appl. Phys. **56**, 05DB04 (2017).
30) R. Vismara, O. Isabella, and M. Zeman, Opt. Express **25**, A402 (2017).
31) T. Sato, H. Hoshida, R. Takabe, K. Toko, Y. Terai, and T. Suemasu, J. Appl. Phys. **124**, 025301 (2018).

© 2020 The Japan Society of Applied Physics